

# 1 True polar wander driven by late-stage volcanism and the 2 distribution of paleopolar deposits on Mars

3

4 Edwin S. Kite<sup>1</sup>, Isamu Matsuyama<sup>1,2</sup>, Michael Manga<sup>1</sup>, J. Taylor Perron<sup>3</sup>, Jerry X. Mitrovica<sup>4</sup>

5

6 1. Earth and Planetary Science, 307 McCone Hall #4767, University of California, Berkeley, CA 94720

7 USA (kite@berkeley.edu)

8 2. Department of Terrestrial Magnetism, Carnegie Institution of Washington, Washington, DC.

9 3. Earth, Atmospheric and Planetary Sciences, MIT, 77 Massachusetts Ave., Cambridge, MA.

10 4. Department of Physics, University of Toronto, 60 St. George Street, Toronto, Ontario, Canada.

11

## 12 **Abstract.**

13 The areal centroids of the youngest polar deposits on Mars are offset from those of adjacent paleopolar  
14 deposits by 5-10°. We test the hypothesis that the offset is the result of true polar wander (TPW), the  
15 motion of the solid surface with respect to the spin axis, caused by a mass redistribution within or on  
16 the surface of Mars. In particular, we consider the possibility that TPW is driven by late-stage  
17 volcanism during the late Hesperian to Amazonian. There is observational and qualitative support for  
18 this hypothesis: in both North and South, observed offsets lie close to a great circle 90° from Tharsis, as  
19 expected for polar wander after Tharsis formed. We calculate the magnitude and direction of TPW  
20 produced by mapped late-stage lavas for a range of lithospheric thicknesses, lava thicknesses, eruption  
21 histories, and prior polar wander events. We find that if Tharsis formed close to the equator, the  
22 stabilizing effect of a fossil rotational bulge located close to the equator leads to predicted TPW of <2°,

23 too small to account for observed offsets. If, however, Tharsis formed far from the equator, late-stage  
24 TPW driven by low-latitude, late-stage volcanism would be  $6\text{-}33^\circ$ , similar to that inferred from the  
25 location of paleopolar deposits. A mass of  $4.4\pm 1.3\times 10^{19}$  kg of young erupted lava can account for the  
26 offset of the Dorsa Argentea Formation from the present-day south rotation pole. This mass is  
27 consistent with prior mapping-based estimates and would imply a mass release of  $\text{CO}_2$  by volcanic  
28 degassing similar to that in the atmosphere at the present time. The South Polar Layered Deposits are  
29 offset from the present rotation pole in a direction that is opposite to the other paleopolar deposits. This  
30 can be explained by either a sequential eruption of late-stage lavas, or an additional contribution from a  
31 plume beneath Elysium. We predict that significant volcanic activity occurred during the time interval  
32 represented by the Basal Unit/Planum Boreum unconformity; Planum Boreum postdates the Promethei  
33 Lingula Lobe; and that the north polar deposits span a substantial fraction of Solar System history. If  
34 the additional contribution to TPW from plumes is small, then we would also predict that Tharsis  
35 Montes formation postdates the the Promethei Lingula Lobe of the South Polar Layered Deposits. We  
36 conclude with a list of observational tests of the TPW hypothesis.

37  
38 **Keywords.** Mars; true polar wander; Hesperian; Amazonian; volcanism; ice-sheets

39  
40 **1. Introduction.**

41 Paleopolar deposits in the polar regions of Mars are not centered on the present spin axis. Although  
42 obliquity changes are probably responsible for the waxing and waning of ice-rich deposits in the  
43 Martian low latitudes (Forget et al., 2006) and mid-latitudes (Head et al., 2006), it has proved  
44 problematic to account for these near-polar offsets using obliquity change. Moderate increases in mean  
45 obliquity (to  $\sim 35^\circ$  from the present  $\sim 25^\circ$ ) extend the latitudinal range over which water ice is stable, but  
46 this expansion should be approximately symmetric about the pole - in contrast with the grossly

47 asymmetric distribution of the paleopolar deposits. At still higher obliquity ( $\geq 40^\circ$ ), all Mars General  
48 Circulation Models (GCMs) predict fast loss of polar water to form a low-latitude ice necklace  
49 (Mischna et al., 2003).

50 Topographic control of atmospheric circulation and ice mass balance has been proposed as an  
51 explanation for the offset of some present-day polar deposits. The low topography of the Hellas and  
52 Argyre impact basins forces a planetary wave which accounts for the offset of the carbon-dioxide  
53 Southern Residual Cap (SRC) from the present-day spin axis (Colaprete et al., 2005). The thickest part  
54 of the southern polar layered plateau underlies the SRC, consistent with topographic control of long-  
55 term water-ice deposition as well. However, Hellas and Argyre are both Noachian ( $> 3.6$  Ga), and the  
56 only significant topographic changes in the Southern Hemisphere since the mid-Hesperian ( $\sim 3.4$  Ga),  
57 in the Tharsis and Syria provinces, could have little effect on either the magnitude or direction of  
58 topographically-controlled asymmetry (Colaprete et al., 2005). In addition, we see a larger pattern  
59 involving offset of both the north and south polar deposits that suggests that the location of the water  
60 ice caps and associated ancient deposits are not due to asymmetric atmospheric effects.

61 We now turn to the alternative hypothesis of late-stage true polar wander, first proposed for the  
62 Martian polar deposits by Murray & Malin (1973). True Polar Wander (TPW) is the movement of a  
63 planet's entire lithosphere with respect to the spin axis in response to changes in mass distribution. Here  
64 we apply TPW theory (Gold, 1955; Goldreich & Toomre, 1969; Willeman, 1984; Matsuyama et al.,  
65 2006) to assess whether relatively recent volcanism in the Martian low- and mid-latitudes could be  
66 responsible, through surface-load driven TPW, for shifts in the distribution of Mars' polar ice sheets  
67 since  $\sim 3.5$  Ga. Because most Martian volcanic and tectonic activity predates  $\sim 3.5$  Gya, we refer to this  
68 as "late-stage" TPW.

69 The basic idea is shown in Figure 1. Lavas postdating the older polar deposits on Mars, but  
70 predating younger polar deposits, change the geoid and so can shift the spin axis and the location of ice

71 accumulation. Late-stage TPW on Mars is a long-standing hypothesis (Murray & Malin, 1973; Schultz  
72 & Lutz, 1988; Tanaka, 2000; Fishbaugh & Head, 2000), but both TPW theory, and Martian geological  
73 and geodetic data, have been refined in recent years and so permit a quantitative analysis. Both surface  
74 and internal loads can drive TPW, but young volcanic loads are more amenable to testing as a possible  
75 driving load because their size and location are relatively well constrained. Our intent is to test if these  
76 geologically plausible loads can produce the required TPW to explain the polar deposit offsets.

77 True Polar Wander of modest magnitude ( $\leq 10^\circ$ ) has been previously suggested to be responsible  
78 for the distribution of both north (Murray & Malin, 1973; Fishbaugh and Head, 2001) and south  
79 (Tanaka, 2000) polar materials. Because the oldest polar materials are Early Amazonian in the north  
80 and Late Hesperian in the south, late-stage TPW requires loading the lithosphere in the Late Hesperian  
81 or Amazonian. By this time the bulk of the Tharsis load, which dominates the Martian geoid, was  
82 already in place (Phillips et al., 2001). However, volcanism has persisted throughout the Amazonian,  
83 resurfacing much of the Tharsis and Elysium regions – 15% of the planet’s surface, of which some  
84 four-fifths lies north of the present-day equator (Nimmo and Tanaka, 2005). The areal centroid of these  
85 lavas is 21N 215E; without other loads they would have driven the pole north along the 215E line. This  
86 is approximately the direction of offset between polar and paleopolar deposits in the north – an  
87 observation that motivates our more detailed study.

88 Here we evaluate the conditions under which TPW driven by recent surface loading may  
89 account for the offset between past and present polar caps. Our scenario complements, but does not  
90 require, proposed TPW events of greater ( $\geq 30^\circ$ ) magnitude and age that have been invoked to solve  
91 geological puzzles earlier in Martian history (e.g. Perron et al., 2007).

92

## 93 **2. The geologic record of polar ice sheets**

94 The residual ice caps at the Martian poles (Herkenhoff et al., 2006) are underlain and abutted by

95 materials that have been mapped as the eroded remnant of past ice-sheet deposits (Figure 2). In the  
96 north, relatively young polar layered deposits (Planum Boreum units of Tanaka et al., 2008),  
97 compositionally dominated by water ice and ~1500m thick, are underlain by older, more lithic-rich  
98 materials (the Basal Unit of Fishbaugh and Head, 2005, platy unit of Byrne and Murray, 2002, lower  
99 unit of Edgett et al., 2003, Rupes Tenuis and Planum Boreum cavi units of Tanaka et al., 2008; we use  
100 the first term), comprising  $\leq 1400\text{m}$  of interbedded layers of sand and fractured ice. Radar sounding  
101 (Phillips et al., 2008) has confirmed the indication from geological mapping (e.g. Fishbaugh & Head,  
102 2005) that the center of these older, more lithic-rich materials is offset from the center of Planum  
103 Boreum by ~300km ( $\sim 5^\circ$ ) along 180E (Figure 2). Near 180E, these sand-rich materials embay and  
104 overlie the Scandia terrain, which bears large rimmed depressions interpreted as dead-ice topography  
105 (Fishbaugh and Head, 2000). To generate these features would require thick ( $> 100\text{m}$ ) and extensive ( $>$   
106  $5 \times 10^4 \text{ km}^2$ ) 'ice sheets', by contrast with the thin ( $\leq 10 \text{ m}$ ) midlatitude icy layers associated with the  
107 recent high-obliquity ice ages (Head et al., 2003). It is unclear how far Scandia morphologies extend  
108 beneath the Basal Unit. If they mark the perimeter of a past ice sheet of similar radius to that of the  
109 Planum Boreum plateau, then its center was offset from the center of Planum Boreum by ~450km (an  
110 additional ~150km) along the 200E line. All of the above units are superposed on the interior Vastitas  
111 Borealis plain, which has an earliest Amazonian crater-retention age by definition (Tanaka, 2005).

112         Still larger offsets are inferred in the south. The  $\text{CO}_2$ -dominated Southern Residual Cap is offset  
113 by  $2.7^\circ$  from the present-day spin axis, and the distribution of the underlying, water-ice Planum  
114 Australe plateau is very asymmetric. A lobe, wedge-shaped in cross-section (Plaut et al., 2007b),  
115 extends in the 180E direction, so that the plateau's areal centroid is at ~85S, although its volumetric  
116 centroid is closer to the pole (Figure 2). Stratigraphic correlation shows that this lobe represents a  
117 subset of Planum Australe's history (the Promethei Lingula Layer sequence of Milkovich & Plaut,  
118 2008). Older and younger sequences within Planum Australe are only found poleward of 80N; this may

119 reflect their original extent, or asymmetric aeolian erosion (e.g., Koutnik et al., 2005). Limning Planum  
120 Australe between longitudes 240E and 105E, and most extensive near 300E and near 10E, is a region  
121 of sinuous, braided ridges and smooth plains punctured by sharp-rimmed depressions, which is mapped  
122 as the Dorsa Argentea Formation (DAF) (Fig. 6b). Radar shows an ice-rich layer extending to 600-  
123 900m depth in this area (Plaut et al., 2007a), supporting the subglacial-melting hypothesis for the DAF  
124 (Head and Pratt, 2001), which has a Hesperian crater-retention age. Radar shows kilometer-deep  
125 depressions beneath Planum Australe resembling the Cavi Angusti within the DAF (Plaut et al., 2007b),  
126 so the DAF likely continues beneath the polar plateau. This interpretation, indicating a paleo-cap offset  
127 by  $\sim 10^\circ$  ( $\sim 600$ km) from the spin axis along the 335E line, is also supported by the pattern of outcrop.

128

### 129 **3. Reorientation of Mars by surface loading**

130 A rotating fluid planet in hydrostatic equilibrium, subject to a superimposed nonequatorial surface load,  
131 reorients to place that mass excess on the equator. However, if a planet has a lithosphere with elastic  
132 strength at spherical harmonic degree two, the equilibrium location of the surface load is not at the  
133 equator, but at an intermediate latitude less than that of loading (Willemann, 1984; Ojakangas and  
134 Stevenson, 1989; Matsuyama et al., 2006, 2007).

135 On Mars, late-stage TPW is also affected by 1) the strong tendency of the preexisting Tharsis  
136 load to remain near the equator (Perron et al., 2007) (all plausible young loads are much smaller than  
137 Tharsis), and 2) the unknown orientation of a fossil equatorial bulge, a “frozen-in” relic of the planet's  
138 spin orientation prior to Tharsis emplacement (Willemann, 1984). Geoid constraints favor solutions  
139 with Tharsis forming close to the equator – in which case the bulge would also lie close to the present-  
140 day equator – but still permit Tharsis to have formed far from the equator, in which case the bulge  
141 would lie at a high angle to today's equator (Daradich et al., 2008). We treat both configurations.

142 We follow Matsuyama et al. (2006) to calculate the inertia tensor perturbations and the

143 corresponding pole position by diagonalizing the inertia tensor. First, we consider the perturbations  
144 associated with the young loads, Tharsis, and the remnant bulge to find the spin-axis orientation prior  
145 to the formation of Tharsis and the young loads. Then, given this initial spin-axis orientation, we  
146 consider the perturbations associated with Tharsis and the remnant bulge alone to calculate the spin-  
147 axis orientation after the formation of Tharsis (Table 1a). We use a standard value for the size of the  
148 geoid perturbation due to the Tharsis load (from Willemann, 1984), although the true value may be  
149 greater or smaller.

150 In practice, Martian volcanism is episodic (Wilson et al., 2001). The viscous relaxation time of Mars  
151 determines whether TPW would also have been episodic, or smoothed. We simplify by considering the  
152 equilibrium response of the planet to a single loading event – equivalent to assuming that the viscous  
153 relaxation time is much shorter than the interval separating younger from older polar deposits.

154

#### 155 **4. Calculation of TPW due to young volcanic loads**

156 We focus on igneous loads emplaced on top of the elastic lithosphere (“surface volcanic loads”) – we  
157 justify this in §6.3). Using geological unit boundaries slightly modified from digitally renovated global  
158 maps (Skinner et al., 2006; Scott and Tanaka, 1986; Greeley and Guest, 1987), we assess the total  
159 thickness of young volcanic materials (lavas, plus relatively shallow intrusions) for each unit (Figure 3;  
160 Table S1).

161 Some units are smooth plains, others are edifices (lobes and cones). We assume uniform  
162 thicknesses for plains lavas, since sub-plains topography is rarely known. Our values resemble those of  
163 Greeley and Schneid (1991). For edifices, we either assume uniform thickness (a late-stage drape over  
164 a Noachian-Early Hesperian core), or truncate near the base (assuming that the majority of the edifice  
165 is late-stage). Planar truncation does not account for the volume of the filled-in flexural pit beneath the  
166 edifice, so the truncated volume underestimates the total edifice volume. There is disagreement over

167 the volume-averaged age of volcanoes that have very young surface ages. For example, Dohm et al.  
168 (2001) reconstruct Olympus Mons as forming in the Late Hesperian/Amazonian, but Werner (2005)  
169 favors formation of Olympus in the Noachian/Early Hesperian. Elastic thickness estimates entail  
170 geothermal gradients generally consistent with late formation (McGovern et al., 2004). However, the  
171 extent to which these estimates are quantitatively reliable is unclear (Belleguic et al., 2005), especially  
172 if volcanoes form above hotspots. To span this uncertainty, we assign 'small', 'medium' and 'large'  
173 thicknesses to each unit (Figure 3; Table S1). We also model TPW driven by drapes of uniform  
174 thickness within the boundary of Late Hesperian/Amazonian volcanic materials given by Nimmo and  
175 Tanaka (2005).

176 [New age estimates and volumes became available as this paper was in revision. Using crater-  
177 counts on High-Resolution Stereo Camera (HRSC) images, Werner (in press) infer that the bulk of the  
178 Tharsis Montes, Olympus Mons, and Elysium were emplaced before the Late Hesperian, although  
179 flank volcanism, caldera activity, and extrusion of flood lavas continued through to the Late  
180 Amazonian. These results suggest that Late Hesperian/Amazonian volcanism can be approximated as a  
181 uniform drape of 100 m to perhaps a few hundred meters thickness, similar to Figure 3a.]

182 Load density  $\rho$  is set to  $3 \times 10^3 \text{ kg m}^{-3}$ . This is conservative for the largest volcanoes (Belleguic et  
183 al., 2005), but overestimates the density of the Medusae Fossae Formation ( $\rho \leq 1.9 \times 10^3 \text{ kg m}^{-3}$ ;  
184 Watters et al., 2007). This error is small compared to the range in thickness estimates. Only that portion  
185 of the load that is uncompensated will drive TPW. For each load, we self-consistently calculate flexure  
186 using fluid Love numbers, and obtain the total geoid perturbation due to the load.

187 We model late-stage TPW for a range of elastic thicknesses ( $T_e$ ), for both the cases where  
188 Tharsis formed close to and far from the equator (Table 1a). Because, once formed, Tharsis must  
189 remain near the equator, the direction of TPW is always close to 160E (90° from the center of Tharsis).  
190 For fixed  $T_e$ , the magnitude of TPW is approximately linear in load volume for reasonably-sized loads.

191 However, it is much greater for the case where Tharsis forms far from the equator than where Tharsis  
192 forms close to the equator; even with the 'large' load, we obtain no more than  $1.6^\circ$  of TPW in the latter  
193 case. This is because the configuration with the fossil rotational bulge at a small inclination to the  
194 present-day equatorial plane is very stable (Perron et al., 2007). For fixed load volume, the extent of  
195 late-stage TPW increases with increasing  $T_e$ , because the level of load compensation decreases; this  
196 effect dominates the increasing magnitude of the remnant rotational bulge, which acts to resist TPW.  
197 Results for drapes of uniform thickness behaved similarly, implying that it is the magnitude of young  
198 volcanism, rather than its exact distribution, that is more important in determining the TPW response.  
199 For simplicity, we assume that the same  $T_e$  characterizes the remnant rotational bulge and the young  
200 volcanic loads.

201 To illustrate the relationship between volcano position and TPW response, we also calculated  
202 the response to the 'large' estimates of volume for individual volcanic provinces (Table 1b). Polar offset  
203 vectors so calculated cannot be meaningfully added, because the TPW response is non-linear.  
204 Apart from Alba Patera, whose effect is to increase the Tharsis load and move Tharsis slightly closer to  
205 the equator, most paleopoles lie along the great circle  $90^\circ$  from Tharsis (Figure 5). The sense of the  
206 shift induced by these volcanic provinces can be understood by inspection of Figure 4. The Medusae  
207 Fossae Formation and Tharsis Montes provinces have volumetric centroids S of the center of Tharsis in  
208 the west-of-Tharsis hemisphere, giving polar shifts in the opposite sense to that of the most voluminous  
209 provinces, which lie N of the equator in the west-of-Tharsis hemisphere. Among these voluminous  
210 provinces, TPW magnitude is strongly dependent on load longitude (Matsuyama et al., 2006). Elysium  
211 is only slightly more massive than Olympus Mons, but because its longitude is close to  $90^\circ$  from  
212 Tharsis it drives a shift  $\sim 3$  times greater than Olympus Mons.

213 Stratigraphic correlations between Elysium and Tharsis are imprecise, although widespread  
214 volcanism on the Elysium rise must have concluded during the Early Amazonian (Tanaka et al., 1992).

215 The consensus among stratigraphers is that overlapping periods of activity occurred at Mars' main late-  
216 stage volcanic centers, rather than sequential eruption at one province followed by another. For all  
217 these reasons, a good starting point when discussing polar wander paths is to assume that the activities  
218 of the Tharsis and Elysium volcanic centers were proportional. However, as will be discussed in §5, our  
219 TPW results illuminate the stratigraphic relations between volcanism and polar activity, allowing us to  
220 reconstruct an alternative 'sequential' history (provided that TPW is in fact responsible for the observed  
221 offsets). This sequence corresponds to the timing of near-surface emplacement of the bulk of the  
222 volume of the volcanoes, not to emplacement of the youngest crater-bearing surfaces.

223

## 224 **5. Comparison with paleopoles inferred from geology**

### 225 **5.1. Geologically inferred paleopoles**

226 Areas of past water ice concentration have been inferred using geology (Tanaka, 2005), and neutron-  
227 spectrometer maps of upper-metre H abundance (Dohm et al., 2007). Although the second dataset may  
228 contain valuable information about ancient ( $\gg 5$  Mya) ice sheets, the possibility that H is present in  
229 salts rather than ice (Basilevsky et al., 2006), and overprinting by recent ( $\leq 5$  Mya) atmosphere-regolith  
230 exchange (Jakosky et al., 2005), complicates interpretation of these shallow materials. We define  
231 paleopolar deposits using topographic and digitized geological data only (Figure 6): Tanaka and Scott  
232 (1987) for the south; Tanaka et al. (2005) for the north. The Scandia formation is mapped (Tanaka et  
233 al., 2005) as being much more extensive than the area of large, rimmed depressions (Scandia Cavi).  
234 Rather than use the entire Scandia formation to define a paleopole, we use Mars Orbiter Laser  
235 Altimeter (MOLA) topography to draw the margins of the Scandia depressions and eskers. A zone of  
236 unusual, large moated domes (Scandia Tholi) encircles the Scandia depressions. These may have been  
237 built up by the extrusion of shallow slurries (Tanaka et al., 2003), and slurry extrusion could occur  
238 without differential loading from an advancing or retreating ice sheet (Kite et al., 2007). But the domes

239 have also been suggested to represent kame-and-kettle topography (Fishbaugh & Head, 2000), so we  
240 use MOLA topography to define their convex hull as a possible paleopolar deposit. We define a single  
241 paleopole using the Olympia dome, which is the only extensive area where the Basal Unit probably lies  
242 close to the surface. This involves the assumption that the part of the Basal Unit making up the bulk of  
243 the Olympia dome is conformable on, or contemporaneous with, the part of the Basal Unit that forms  
244 the base of Planum Boreum (Fishbaugh & Head, 2005); however, Tanaka et al. (2008) argue that the  
245 first part is separated from the second by a major unconformity.

246         Polar caps are centered close to the spin axis today (average deviation  $2.4^\circ$ , Table 2), and are  
247 likely to have tracked the spin axis in the past, at least during conditions of low ( $<40^\circ$ ) obliquity. We  
248 show the distance between young polar caps and the present-day spin axis in Figure 6, by dashed lines  
249 bracketing the calculated polar wander track. This is our estimate of the 'proxy error' involved in using  
250 polar caps as proxies for the location of the spin axis. Radar indicates that the Basal Unit continues  
251 under much of Planum Boreum (Putzig et al., 2008), and the spatial distribution of Dorsa Argentea  
252 Formation outcrop strongly suggests that it continues under the thickest part of Planum Australe.  
253 Therefore, the areal centroid of present-day outcrop of a paleopolar deposit cannot be considered a  
254 paleopole. Instead, we approximate past ice sheets by circles, and define a simple penalty function to  
255 evaluate the goodness of fit of a given circular planform to geological boundaries. Incorrect inclusion  
256 of non-paleopolar material and exclusion of paleopolar material both score +1 per grid cell ( $\sim 9\text{km}^2$ ),  
257 and correct inclusion of paleopolar material is rewarded with a score of -1 per cell. Overlying materials  
258 are masked out and not scored. We then define the paleopole for a given geological unit to be the center  
259 of the circular ice-sheet with the minimum score, searching systematically over cap latitude and  
260 longitude. The circle that best fits Olympia Planum matches the area of Basal Unit independently  
261 mapped by radar (Putzig et al., 2008), lending credence to our assumption that paleopolar caps were  
262 approximately circular. We do not attempt a formal error estimate for the paleocenter locations: this

263 would have to take into account incomplete geological preservation, mapping imprecision, non-circular  
264 ice sheets, and possible asymmetric retreat. We consider that these effects introduce an error in  
265 assigning a centroid location to a paleopolar deposit comparable to the 'proxy error' defined above. This  
266 additional 'measurement error' is shown by the outer green circles in Figure 6.

267 In the north, we only consider past ice-sheets with radii equal to that of present-day Planum  
268 Boreum (Greenwood et al., 2008). We find best-fitting pole locations for the Olympia dome, for the  
269 Scandia depressions, and for the Scandia depressions and mounds taken together (Table 1a). Ice  
270 outliers, large areas of perennially high albedo south of the Olympia dome, bracket the polar wander  
271 path associated with progressive emplacement of a volcanic load (§4; Figure 6a). They have only  
272 superficial topographic expression, and their age is uncertain. They may be recent deposits unrelated to  
273 the Scandia depressions, in which case it would be inappropriate to fit them. Alternatively, if they are  
274 outliers of a formerly more extensive polar plateau (Zuber et al., 1998), then they should be weighted  
275 when defining paleopoles. We plot only the first possibility, which we consider more likely because the  
276 ice outliers superpose most other deposits (Table 1a; Figure 6) and are still annually frosting and  
277 defrosting (Calvin and Titus, 2008). The calculated polar wander path including the ice outliers (not  
278 shown) runs along  $180(\pm 10)^\circ$ E.

279 Taken together, our paleopoles in the north define a polar wander path of magnitude  $(5\pm 2)^\circ$   
280 (Figure 6a). This increases to  $(7\pm 2)^\circ$  if the enigmatic Scandia mounds also indicate ice-sheet processes.  
281 The Basal Unit paleopole is almost as close to the spin axis as is the upper part of Planum Boreum, so  
282 TPW is only one of several possible explanations for the offset of the Basal Unit from the spin axis and  
283 from the center of the upper part of Planum Boreum. For example, pre-existing (and now-buried)  
284 topography could have seeded growth of an ice-sheet. Subsequently, the Basal Unit topographic rise  
285 might have shifted atmospheric circulation to favor off-center deposition of younger volatile-rich  
286 deposits.

287 In the south, caps with radius equal to that of Planum Australe cannot give a good fit to the  
288 location of the DAF. When we allow the paleo-ice-sheet radius to increase, we obtain a much more  
289 satisfactory fit. This may be because the Martian surface lost water between DAF time and Scandia  
290 time (Kulikov et al., 2007), so that the DAF ice-sheet was more voluminous. In addition, higher  
291 lithospheric heat flux (Solomon et al., 2005) may have permitted the ice-sheet to flow downslope,  
292 leading to a noncircular planform and greater width:height ratio. Geological syntheses based on image  
293 interpretation (Ghatan & Head, 2004) suggest that the DAF ice-sheet was at least locally hydrologically  
294 active, indicating a bed temperature near the pressure melting point. This would have permitted much  
295 more rapid ice creep than within the present-day polar layered deposits (Goldsby & Kohlstedt, 2001).  
296 Bedrock topography in the south polar region favors asymmetric accumulation and flow: it is more  
297 rugged, and has steeper long-baseline tilts, than the north polar region (Plaut et al., 2007b). The best-  
298 fitting ice sheet, with radius 1020 km (q.v. 700 km for Planum Australe), is centered along our  
299 calculated TPW path. Its offset relative to the present-day spin axis is  $7.9^\circ$ , and we use this value in the  
300 Discussion. However, given the importance of Southern Hemisphere topography in controlling  
301 precipitation patterns near the south pole, it is arguably better to measure the offset relative to the SRC  
302 ( $5.2^\circ$ ). In this case, the volume of volcanism needed to generate TPW is reduced by 1/3, but our  
303 conclusions are not qualitatively affected.

304

## 305 **5.2 Assessment of the late-stage TPW hypothesis**

306 In Figure 6 we compare paleopole locations inferred from geological constraints (Table 1a) to those  
307 computed using loading theory (Table 1a). As episodic volcanism progressively emplaced the young  
308 volcanic load, the magnitude of TPW would have increased. Therefore older paleopolar deposits should  
309 show progressively larger offsets from the present-day spin axis, a prediction that matches observations  
310 (Figure 6) and correlations between north and south (Figure 7).

311 If Tharsis formed close to the equator, volcanically-driven TPW can explain at most the location  
312 of the Basal Unit, even with the ‘large’ estimated volcanic load. Accounting for the older deposits  
313 requires instead that Tharsis formed far from the equator. In that case, even the 'small' load gives TPW  
314 sufficient to explain the offset between the present-day spin axis and the DAF.

315 The trend of the paleopoles in the north clearly deviates from the great circle  $90^\circ$  from Tharsis  
316 (Figure 6a). However, Paleopoles 1 – 2 (which lie close to the great circle  $90^\circ$  from Tharsis) are more  
317 reliable than Paleopole 3 (which does not) because of the greater area of outcrop of the Planum Boreum  
318 and the Basal Unit compared to that of the Scandia depressions. Fitting caps to relatively small  
319 outcrops introduces additional uncertainty into the pole calculation. In turn, Paleopoles 1-3 are much  
320 more reliable than Paleopole 4 (the biggest outlier), because we do not know what created the Scandia  
321 Tholi. Moreover, the ice outliers, which are thickest in the 110E–180E sector, might mute topographic  
322 evidence for ice-sheet action to the west of our paleopoles, introducing an eastward bias in paleopole  
323 longitude. Therefore, we consider the distribution of paleopolar deposits in the north polar region  
324 consistent with TPW, although certainly not compelling when considered in isolation.

325 In the south, all geologically-inferred paleopoles lie along our calculated polar wander path  
326 (Figure 6b). As expected given its greater age, the DAF shows a larger offset from the present-day spin  
327 axis than does the Basal Unit. The center of Planum Australe lies along our calculated TPW path, but in  
328 the opposite direction from that expected for proportional emplacement of young volcanic loads (§5.3).

329 Given the plausibility of our input parameters, and the acceptable match between observed and  
330 calculated polar wander magnitudes and directions, we favor the late-stage TPW explanation for the  
331 distribution of paleopolar deposits on Mars. However, if later research confirms that Tharsis in fact  
332 formed close to the equator, this will rule out TPW driven by surface loads as an explanation for the  
333 distribution – unless late-stage Martian magmatism was much more voluminous than in current models.  
334 Gravity data to degree and order 2 are better fit by a small-TPW scenario than by a large-TPW scenario

335 (Daradich et al., 2008), but that work did not consider loads other than Tharsis and the fossil rotational  
336 bulge (such as internal loads, or the late-stage surface loads considered in this paper). More detailed  
337 modeling of gravity anomalies and geodynamic history might help to constrain the latitude at which  
338 Tharsis formed.

339

### 340 **5.3. Example integrated volcanic and polar history of Late Hesperian/Amazonian Mars**

341 Because Tharsis dictates the path of late-stage TPW, our inferred TPW path cannot be used to infer the  
342 exact location of its causative loads (Figure 4). For example, the difference in polar wander direction  
343 for TPW driven by Elysium versus Olympus is negligible, despite the  $>70^\circ$  of longitude separating  
344 Elysium and Olympus. The longitude resolution of our geologically inferred paleopoles is also poor, so  
345 we cannot constrain load longitude much better than by quadrant (Figure 4). However, in combination  
346 with upper limits on load volume from MOLA topography, and lower limits on unit age from crater  
347 counts, we identify a possible sequence of volcanic loading episodes and pole shifts, and polar  
348 deposition episodes (Figure 7).

349         The sequence starts with deposition of the Dorsa Argentea Formation in the Late Hesperian. The  
350 Elysium rise is already partly in place (Figure 7a). Waning Elysium activity, increasingly supplemented  
351 by proto-Olympus Mons, drives the pole  $\sim 5.5^\circ$  towards 335E (towards the hemisphere centered on the  
352 Martian meridian) during Scandia and prior to Basal Unit time (Figure 7b). The top of the Basal Unit  
353 marks a major unconformity in the north. Olympus Mons and Arcadia flood lavas move the pole a  
354 further  $\sim 8.1^\circ$  meridian-ward,  $\sim 5.7^\circ$  beyond its present location. The Promethei Lingula Lobe of the  
355 South Polar Layered Deposits forms after this loading event (Figure 7c). Next, the locus of volcanism  
356 shifts east to the Tharsis Montes, reversing the sign of TPW and bringing the spin axis to its present  
357 configuration. Thicker lithosphere allows a given load to produce a greater geoid anomaly, so cooling  
358 of the planet enhances TPW during this final stage. Planum Boreum is deposited during this TPW

359 event, a  $\sim 5.7^\circ$  shift in the anti-meridian direction (Figure 7d), accounting for its offset from the present-  
360 day north rotation pole (Figure 6a). The Medusae Fossae Formation, Syria and Alba play subsidiary  
361 roles (Figure 5).

362 This sequence of events assumes there has been little change in the contribution to the geoid  
363 from internal loads and dynamic topography over the past  $\sim 3.5$  Gyr. In §6.3, we relax this assumption,  
364 and suggest that construction of the Elysium province, followed by cessation of plume activity beneath  
365 Elysium, is an alternative and perhaps simpler explanation of the observations. If late-stage volcanism  
366 at the Tharsis Montes has been volumetrically minor (Werner, in press), late-stage Tharsis Montes  
367 volcanism would have been insufficient to generate the  $\sim 5.7^\circ$  shift in the anti-meridian direction shown  
368 in Figure 7d, and a contribution from internal loads would be required to explain this step of Mars'  
369 inferred TPW history.

370

## 371 **6. Discussion**

### 372 **6.1. Implications for rates of melting and degassing**

373  $T_e$  is probably  $\geq 300$  km today (Phillips et al., 2008), but was  $93 \pm 40$  km at the time of Olympus Mons  
374 emplacement (Belleguic et al., 2005). Given the decay of the mantle's radiogenic heat source, the  
375 relevant  $T_e$  is probably close to  $\sim 100$  km, the value for the Early Amazonian when most of the load  
376 would have been emplaced.

377 Given the  $\sim$ linear relationship between load volume and magnitude of TPW (Table 1a) for  
378 geologically defensible loads, we can use geologically inferred TPW to estimate the subsequent volume  
379 of volcanism (Figure 8). For example, taking the Dorsa Argentea Formation to be  $\sim 3.6$  Ga old  
380 (Hartmann, 2005), the average rate of volcanism since is  $(4.1 \pm 1.2) \times 10^{-3} \text{ km}^3 \text{ yr}^{-1}$ . This is less than the  
381 pre-MOLA estimate of Greeley and Schneid (1991),  $7.3 - 14.6 \times 10^{-3} \text{ km}^3 \text{ yr}^{-1}$ , but matches thermal  
382 evolution models (O'Neill et al., 2007).

383           With an estimate of the CO<sub>2</sub> content of Martian magma – 516 mg/kg (O'Neill et al., 2007), with  
384 large uncertainties (Hirschmann and Withers, 2008) – we can estimate total late-stage volatile release to  
385 the atmosphere. For the case where Tharsis forms far from the equator, and T<sub>e</sub> = 100km, (4.4±1.3) x10<sup>19</sup>  
386 kg magma (which, if completely degassed, would have released 5.8±1.8 mbar CO<sub>2</sub>) should have been  
387 extruded since DAF time, and (2.8±1.3) x10<sup>19</sup> kg magma (which, if completely degassed, would have  
388 released 3.6±1.7 mbar CO<sub>2</sub>) since the Scandia depressions formed. This falls to 3.3±1.0 mbar and  
389 2.1±1.0 mbar respectively if with T<sub>e</sub> = 200 km. Quoted errors consider only the error in paleopole  
390 positions, not in T<sub>e</sub>. Our best-estimate of total late stage degassing, ~6 mbar, is also the size of the  
391 present-day near-surface CO<sub>2</sub> reservoir (6.4 mbar in the atmosphere, and 0.4 mbar in the SRC).

392           Present-day Martian atmospheric pressure reflects the balance of Late Hesperian/Amazonian  
393 volcanic degassing and atmospheric loss, added to whatever atmosphere was inherited from 'early  
394 Mars'. The inherited atmosphere would have been very tenuous if the active young Sun drove CO<sub>2</sub> loss  
395 rates greatly in excess of volcanic degassing rates during the Noachian/Early Hesperian (Manning et  
396 al., 2006). In that case, the rough equivalence of TPW-derived volcanic degassing estimates and  
397 present-day atmospheric pressure would require that atmospheric loss rates were smaller than volcanic  
398 degassing rates, integrated over the Late Hesperian/Amazonian. In other words, long-term average  
399 atmospheric mass and globally-averaged surface temperature may have been *increasing* over the last  
400 three-quarters of Martian history, with important implications for geomorphology and the likelihood of  
401 surface liquid water (see also Richardson & Mischna, 2005). The requirement that atmospheric loss  
402 rates be small is consistent with the paucity of carbonates on the Martian surface (Bibring et al., 2006),  
403 and with Mars Express measurements of present-day atmospheric escape rates – which are equivalent  
404 to only 0.2 – 4 mbar CO<sub>2</sub> extrapolated over 3.5 Ga (although not all processes have been quantified)  
405 (Barabash et al., 2007).

406

407 **6.2. Are Planum Boreum and Planum Australe old enough to have experienced TPW?**

408 Our proposed TPW scenario implies an age for Planum Australe and the upper part of Planum Boreum  
409 that is older than some estimated ages, but consistent with others. If they formed recently (e.g., <5 Myr  
410 in the North; Phillips et al., 2008), geologically detectable TPW is unlikely to have occurred since.  
411 TPW acts to filter out high temporal frequencies, and the only non-polar changes in surface load since  
412 5 Mya have been the emplacement of thin (Campbell et al., 2007) lavas, perhaps the uppermost  
413 member of the Medusae Fossae Formation (Watters et al., 2007), and perhaps partial sublimation of  
414 non-polar icy deposits (Head et al., 2006). Collectively, these load changes could have produced only  
415 minor TPW. However, estimating the age of icy deposits is difficult, because sublimation of overburden  
416 may remove craters, and crater topography possibly undergoes viscous relaxation. The largest craters,  
417 though few in number, imply a surface age of >330 Myr for the upper part of Planum Boreum, and  
418 >500 Myr for Planum Australe (Pathare et al., 2005). Because the stratigraphy of the north polar  
419 layered deposits cannot yet be definitively linked with a known time scale (Perron and Huybers, 2009),  
420 it remains possible that the upper part of Planum Boreum is significantly older than a few million years.  
421 Therefore, either or both Planum Australe and the upper part of Planum Boreum may be old enough to  
422 have undergone geologically measurable TPW, which may help to explain the offset of their areal  
423 centers from the present-day spin axis.

424

425 **6.3. Other loads**

426 If mantle plumes underlie Tharsis and Elysium, they may have changed intensity (O'Neill et al., 2007)  
427 or position over time. However, the geoid anomaly at degree 2 (the wavelength relevant to TPW)  
428 produced by a plume of constant flux and position changes little as the lithosphere thickens over time  
429 (Roberts and Zhong, 2004). Rouby et al. (2008) show that plume initiation could have led to 1-15° of  
430 TPW on pre-Tharsis Mars, setting aside stabilization by the fossil rotational bulge.

431 Extensive volcanism on the Elysium rise ceased in the Early Amazonian (Tanaka et al., 1992).  
432 The decline of volcanic activity may correspond to a waning of plume activity beneath Elysium. If so,  
433 then the 'overshoot and rebound' relative to today's spin-axis recorded by the locations of the polar  
434 deposits could be due solely to Elysium. Our reasoning is as follows. On Mars, the geoid anomaly due  
435 to mantle plumes at wavelengths appropriate for Elysium is probably positive (upwards), though small  
436 (Roberts and Zhong, 2004); the positive anomaly due to dynamic topography supported by the rising  
437 mantle exceeds the negative anomaly due to the low-density mantle forming the plume. Therefore, with  
438 plume-supported volcanism, the combination of a dynamic, internal load and a growing surface load  
439 induces greater TPW than the surface load alone. This could correspond to the evolution from a) to c)  
440 in Figure 7 (the 'overshoot') . Removal of the internal load, for example by a waning plume, is in effect  
441 a negative load. This could correspond to the evolution from c) to d) in Figure 7 (the 'rebound').

442 Polar wander driven by dust, ice, or material deposited by the waning circum-Chryse outflows  
443 was probably small compared to the volcanically-driven wander assessed here. The thin Vastitas  
444 Borealis outflow channel deposits certainly predate the Scandia terrain, and probably largely predate  
445 the Dorsa Argentea Formation. The TPW contribution of the ice sheets themselves would have been  
446 minor unless vastly more ice was available for atmospheric transport in the past than at present.

447 On Earth, basalt underplating the low-density crust during plume impingement may match or  
448 exceed erupted volumes (Cox, 1995). Such 'bottom loading' on Mars would complicate our analysis.

449 We cannot distinguish between true polar wander of the lithosphere-plus-mantle relative to the  
450 spin axis, and differential motion of the lithosphere with respect to the mantle. Our calculations in §3  
451 assume the former. The alternative has recently been proposed (Zhong, 2009), and would lead to very  
452 different implications for Martian volcanic (and climatic?) history.

453

#### 454 **6.4 Further tests**

455 We have established the plausibility of geologically significant late-stage TPW on Mars, but our  
456 conclusions depend on assumptions about the volcanic and polar history of Mars that need to be tested.  
457 The TPW hypothesis would be disfavored if analysis of crater size-frequency distributions showed a  
458 Noachian/Early Hesperian density of buried craters at shallow depths throughout the area of young  
459 volcanism. Provided that the intrusive:extrusive volume ratio is comparable to terrestrial values (~5:1;  
460 White et al., 2006), this could bound the volume of late-stage near-surface loads as less than required to  
461 drive the proposed TPW. On the other hand, tectonic mapping might reveal patterns of fault  
462 reactivation parsimoniously explained by lithospheric stresses due to late-stage TPW (Melosh, 1980).  
463 Our best-fitting Scandia paleopoles imply that features similar to the Scandia rimmed depressions  
464 extend under Planum Boreum about as far as the present-day spin axis. This predicts that the basal  
465 interface of the Basal Unit should have hundreds of meters of relief at 10km – 100km scales,  
466 contrasting with the low ~10km-scale roughness of the basal interface of Gemini Lingula (Phillips et  
467 al., 2008) and of Vastitas Borealis (Kreslavsky & Head, 2000). If radar shows these features to be  
468 absent, asymmetric retreat of a formerly more extensive ice sheet (Fishbaugh & Head, 2001) may be a  
469 better explanation for the Scandia features.

470 Our late-stage TPW scenario alters the topographic boundary conditions for Noachian/Early  
471 Hesperian climate by 1) removing volcanic edifices, and 2) shifting zonal climatic belts relative to the  
472 lithosphere. Ventifacts at the mid-Hesperian Mars Pathfinder (MPF) landing site are oriented oblique to  
473 the strongest present-day winds (Greeley et al., 2000); this cannot be accounted for by obliquity change  
474 (Fenton & Richardson, 2001; Haberle et al., 2003). If a GCM using the altered topographic boundary  
475 conditions provided by our TPW scenario yields strong winds at the MPF site which parallel the  
476 observed ventifacts, the hypothesis of late-stage TPW would be supported.

477 Also, if the significant offset between the centers of the Basal Unit and the upper NPLD is due  
478 to TPW, the Basal Unit must predate a substantial fraction of Late Hesperian / Amazonian volcanism.

479 Given that a recent surge in volcanism is unlikely (but not impossible), this entails a mid-Amazonian or  
480 earlier Basal Unit age. Consequently, we predict that the north polar deposits span a substantial fraction  
481 of Solar System history. If Martian polar stratigraphy records orbitally forced variations in insolation  
482 (Montmessin, 2006), then the polar deposits of Mars might greatly extend the time range over which  
483 geology constrains orbital dynamics (Olsen and Kent, 1999).

484

## 485 **7. Conclusions**

486 Late Hesperian/Early Amazonian paleopolar deposits near the Martian poles are offset from the  
487 present-day poles in a manner inconsistent with simple obliquity change. We find that true polar  
488 wander driven by late-stage, low-latitude volcanic loads can account for these observations, if (and  
489 only if) Tharsis formed far from the equator. Gravity data favor scenarios where Tharsis forms close to  
490 the equator, but permit scenarios where Tharsis forms far from the equator (Daradich et al., 2008).

491 Three of the four paleopolar deposits on Mars can be explained by proportional emplacement of  
492 volcanic load, but the South Polar Layered Deposits cannot be explained in this way. The SPLD  
493 paleopole can, however, be accounted for if the Tharsis Montes postdate the South Polar Layered  
494 Deposits or if internal (plume-related) loads changed with time. By linking widely separated TPW-  
495 inducing and pole-tracking deposits, TPW permits a new method of stratigraphic correlation that is  
496 independent of crosscutting relationships and crater counts.

497 Our calculations illustrate (Fig. 7) that the locations of *all* of the paleopolar deposits near the  
498 Martian poles could be the result of TPW, but our confidence level is high for only one of the four  
499 deposits, the Dorsa Argentea Formation. Younger deposits are closer to the present-day spin axis, and it  
500 is possible that meteorological factors are responsible for their offset from the pole. This could be  
501 studied with a GCM of sufficient resolution ( $\sim 1^\circ$  in latitude).

502 The hypothesis of true polar wander driven by late-stage volcanism survives our test.

503 **References**

- 504 Barabash, S., A. Federov, R. Lundin, and J.-E. Sauvaud (2007), Martian atmospheric erosion rates,  
505 Science 315, 501-503.  
506
- 507 Basilevsky, A.T., et al. (2006), Search for causes of the low epithermal neutron flux anomaly in the  
508 Arabia Terra region (Mars), Solar System Research 40(5), 355-374  
509
- 510 Belleguic V., P. Lognonne, and M. Wieczorek (2005), Constraints on the Martian lithosphere from  
511 gravity and topography data, J. Geophys. Res. 110(E11), doi:10.1029/2005JE002437.  
512
- 513 Bibring, J.-P., et al. (2006), Global Mineralogical and Aqueous Mars History Derived from  
514 OMEGA/Mars Express Data, Science 312, 400-404.  
515
- 516 Bradley, B.A., S.E.H. Sakimoto, H. Frey, and J.R. Zimbelman (2002), Medusae Fossae Formation:  
517 New perspectives from Mars Global Surveyor, J. Geophys. Res. 107(E8), doi:10.1029/2001JE001537.  
518
- 519 Byrne, S., and B.C. Murray (2002), North polar stratigraphy and the paleo-erg of Mars, J. Geophys.  
520 Res., 107(E6), 5044.  
521
- 522 Calvin, W.M., and T.N. Titus (2008), Summer season variability of the north residual cap of Mars as  
523 observed by the Mars Global Surveyor Thermal Emission Spectrometer (MGS-TES), Planetary and  
524 Space Science, 56, 212-226.  
525
- 526 Campbell, B.A., et al. (2007). SHARAD mapping of subsurface geological horizons in Amazonis  
527 Planitia. 7<sup>th</sup> International conf. on Mars, abs. #3225.  
528
- 529 Colaprete, A., J.R. Barnes, R.M. Haberle, J.L. Hollingsworth, H.H. Kieffer, & T.N. Titus (2005),  
530 Albedo of the south pole on Mars determined by topographic forcing of atmosphere dynamics, Nature  
531 435, 184-188.  
532
- 533 Cox, K.G. (1995), Continental magmatic undeplating, Phil. Trans. Roy. Soc. A., 342, 155-166.  
534
- 535 Daradich, A., et al. (2008), Equilibrium rotational stability and figure of Mars, Icarus 194, 463-475.  
536
- 537 Dohm, J.M., et al. (2001), Ancient drainage basin of the Tharsis region, Mars, J. Geophys. Res.  
538 106(E12), 32,943–32,958.  
539
- 540 Dohm, J.M., et al. (2007), Possible ancient giant basin and related water enrichment in the Arabia Terra  
541 province, Mars, Icarus 190, 74-92.  
542
- 543 Edgett, K.S., R.M.E. Williams, M.C. Malin, B.A. Cantor, and P.C. Thomas (2003), Mars landscape  
544 evolution: influence of stratigraphy on geomorphology in the north polar region, Geomorphology 52,  
545 289-297.  
546
- 547 Fenton, L., and M.I. Richardson (2001), Martian surface winds: Insensitivity to orbital changes  
548 and implications for aeolian processes. J. Geophys. Res. 106(E12), 32,885-32,902.

549  
550 Fishbaugh, K.E. and J.W. Head (2000), North polar region of Mars: Topography of circumpolar  
551 deposits from Mars Orbiter Laser Altimeter (MOLA) data and evidence for asymmetric retreat of the  
552 polar cap, *J. Geophys. Res.* 105(E9), 22,455-22,486.  
553  
554 Fishbaugh, K.E., and J.W. Head (2001), Comparison of the north and south polar caps of Mars, *Icarus*  
555 154, 145-161.  
556  
557 Fishbaugh, K.E., and J.W. Head (2005), Origin and characteristics of the Mars north polar Basal Unit  
558 and implications for polar geologic history, *Icarus* 174, 444-474.  
559  
560 Forget, F., R.M. Haberle, F. Montmessin, B. Levrard, & J. W. Head (2006), Formation of glaciers on  
561 Mars by atmospheric precipitation at high obliquity, *Science* 311, 368-371.  
562  
563 Ghatan, G.J., and J.W. Head III (2004), Regional drainage of meltwater beneath a Hesperian-aged  
564 south circumpolar ice sheet on Mars, *J. Geophys. Res.* 109, doi:10.1029/2003JE002196.  
565  
566 Gold, T., (1955), Instability of the Earth's axis of rotation, *Nature* 175, 526– 529.  
567  
568 Goldreich, P., and A. Toomre (1969), Some remarks on polar wandering, *J. Geophys. Res.*, 74, 2555–  
569 2567  
570  
571 Goldsby, D.L., and D.L. Kohlstedt (2001), Superplastic deformation of ice: Experimental observations,  
572 *J. Geophys. Res.* 106(B6), 11,017–11,030.  
573  
574 Greeley, R., and J.E. Guest (1986), Geological Map of the Western Equatorial Region of Mars, US  
575 Geol. Surv. Scientific Investigations I-1802-B  
576  
577 Greeley, R., and B.D. Schneid (1991), Magma generation on Mars: Amounts, rates, and comparisons  
578 with Earth, Moon and Venus, *Science* 254, 996-998.  
579  
580 Greeley, R., M.D. Kraft, R.O. Kuzmin, and N.T. Bridges (2000), Mars Pathfinder landing site:  
581 Evidence for a change in wind regime from lander and orbiter data, *J. Geophys. Res.* 105(E1), 1829-  
582 1840.  
583  
584 Greenwood, J.P., et al. (2008), Hydrogen isotope evidence for loss of water from Mars through time,  
585 *Geophys. Res. Lett.*, doi:10.1029/2007GL032721, in press.  
586  
587 Haberle, R.M., J.R. Murphy and J. Schaeffer (2005), Orbital change experiments with a Mars general  
588 circulation model, *Icarus* 161(1), 66-89.  
589  
590 Hartmann, W.K., (2005), Martian cratering 8: Isochron refinement and the chronology of Mars, *Icarus*  
591 174(2), 294-320.  
592  
593 Head, J.W., et al. (2003), Recent ice ages on Mars, *Nature* 426, 797-802.  
594  
595 Head, J.W., and S. Pratt (2001), Extensive Hesperian-aged south polar ice sheet on Mars: Evidence for

596 massive melting and retreat, and lateral flow and ponding of meltwater, *J. Geophys. Res.* 106(E5),  
597 12275-12299.  
598  
599 Head, J.W., et al. (2006), Extensive valley glacier deposits in the northern mid-latitudes of Mars:  
600 Evidence for Late Amazonian obliquity-driven climate change, *Earth Planet. Sci. Lett.* 241, 663-671.  
601  
602 Herkenhoff, K., S. Byrne, and K.L. Tanaka (2006), Mars polar geologic nomenclature: What are the  
603 caps? In: 4<sup>th</sup> Mars Polar Sci. Conf. Abstract 8034.  
604  
605 Hirschmann, M.M., and A.C. Withers (2008), Ventilation of CO<sub>2</sub> from a reduced mantle and  
606 consequences for the early Martian greenhouse, *Earth and Planet. Sci. Lett.* 270, 147-155.  
607  
608 Ivanov, M.A., and J.W. Head III (2006). Alba Patera, Mars: Topography, structure, and evolution of a  
609 unique late Hesperian–early Amazonian shield volcano, *J. Geophys. Res.*, 111, E09003,  
610 doi:10.1029/2005JE002469.  
611  
612 Jakosky, B., M.T. Mellon, E.S. Varnes, W.C. Feldman, W.V. Boynton, and R.M. Haberle (2005), Mars  
613 low-latitude neutron distribution: Possible remnant near-surface water ice and a mechanism for its  
614 recent emplacement, *Icarus* 175, 58-67.  
615  
616 Kite, E.S., N. Hovius, J.K. Hillier, and J. Besserer (2007), Candidate mud volcanoes in the northern  
617 plains of Mars, American Geophysical Union, Fall Meeting 2007, abstract #V13B-1346.  
618  
619 Koutnik, M.R., S. Byrne, B.C. Murray, A.D. Toigo, and Z.A. Crawford (2005), Eolian controlled  
620 modification of the martian south polar layered deposits, *Icarus* 174(2), 490-501.  
621  
622 Kreslavsky, M.A., and J.W. Head III (2000), Kilometer-scale roughness of Mars: results from MOLA  
623 data analysis. *J. Geophys. Res.* 105(E11), 26695-26711.  
624  
625 Kulikov, Y.N., et al. (2007), A comparative study of the influence of the active young sun on the early  
626 atmospheres of Earth, Venus, and Mars, *Space Sci. Rev.* 129, 207-243.  
627  
628 McGovern, P. J., et al. (2004), Correction to “Localized gravity/topography admittance and correlation  
629 spectra on Mars: Implications for regional and global evolution”, *J. Geophys. Res.*,  
630 doi:10.1029/2004JE002286.  
631  
632 Manning, C.V., C.P. McKay, and K.J. Zahnle (2006), Thick and thin models of the evolution of carbon  
633 dioxide on Mars, *Icarus* 180, 38-59.  
634  
635 Matsuyama, I., et al. (2006), Rotational stability of dynamic planets with elastic lithospheres, *Journal*  
636 *of Geophysical Research* 111(E2), E02003.  
637  
638 Matsuyama, I., F. Nimmo, and J.X. Mitrovica (2007), Reorientation of planets with lithospheres: The  
639 effect of elastic energy, *Icarus* 191(2), 401-412.  
640  
641 Melosh, H.J. (1980), Tectonic patterns on a reoriented planet: Mars, *Icarus* 44, 745-751.  
642

643 Milkovich, S.M., and J.J. Plaut (2008), Martian South Polar Layered Deposit stratigraphy and  
644 implications for accumulation history, *J. Geophys. Res.*, 113, E06007, doi:10.1029/2007JE002987.  
645

646 Mischna, M.A., M.I. Richardson, R.J. Wilson and D.J. McCleese (2003), On the orbital forcing of  
647 martian water and CO<sub>2</sub> cycles: A general circulation model study with simplified volatile schemes. *J.*  
648 *Geophys. Res.*, 108(E6) 5062, doi:10.1029/2003JE002051.  
649

650 Montmessin, F. (2006), The orbital forcing of climate changes on Mars, *Space Sci. Rev.* 125, 457-472.  
651

652 Murray, B.C., and M.C. Malin (1973), Polar wandering on Mars?, *Science* 179, 997-1000.  
653

654 Nimmo, F., and K.L. Tanaka (2005), Early crustal evolution of Mars, *Annual Review of Earth and*  
655 *Planetary Sciences* 33, 133-161.  
656

657 Ojakangas, G.W., and D.J. Stevenson (1989), Polar wander of an ice shell on Europa, *Icarus* 81, 242-  
658 270.  
659

660 Olsen, P.E., and D.V. Kent (1999), Long-period Milankovitch cycles from the Late Triassic and Early  
661 Jurassic of eastern North America and their implications for the calibration of the Early Mesozoic time-  
662 scale and the long-term behaviour of the planets, *Phil. Trans. Roy. Soc. A*, 357, 1761-1786.  
663

664 O'Neill, C., A. Lenardic, A.M. Jellinek, and W.S. Kiefer (2007), Melt propagation and volcanism in  
665 mantle convection simulations, with applications for Martian volcanic and atmospheric evolution, *J.*  
666 *Geophys. Res.* 112(E7), doi:10.1029/2006JE002799.  
667

668 Pathare, A., D. A. Paige, and E. Turtle (2005), Viscous Relaxation of Craters within the Martian South  
669 Polar Layered Deposits, *Icarus*, 174, 396-418.  
670

671 Perron, J.T., et al. (2007), Evidence of an ancient martian ocean in the topography of deformed  
672 shorelines. *Nature*, 447, 840-843.  
673

674 Perron, J.T., and P. Huybers (2009), Is there an orbital signal in the polar layered deposits on Mars?,  
675 *Geology*, 37, 155-158, 10.1130/G25143A.1.  
676

677 Phillips, R.J., et al. (2001), Ancient geodynamics and global-scale hydrology on Mars, *Science* 291,  
678 2587-2591.  
679

680 Phillips, R.J., et al. (2008), Mars North Polar Deposits: stratigraphy, age, and geodynamical response,  
681 *Science* 320, 1182-1185.  
682

683 Plaut, J., et al. (2007a), Radar sounding of subsurface layers in the South Polar plains of Mars, *LPSC*  
684 38, 2144.  
685

686 Plaut, J., et al. (2007b), Subsurface Radar Sounding of the South Polar Layered Deposits of Mars,  
687 *Science* 316, 92-95.  
688

689 Putzig, N.E., et al. (2008), Stratigraphic mapping of the north polar layered deposits on Mars from

690 radar soundings, *Lunar Planet Sci. Conf.* 39, 2355.  
691  
692 Richardson, M.I., and M.A. Mischna (2005), Long-term evolution of transient liquid water on Mars, *J.*  
693 *Geophys. Res.* 110, doi:10.1029/2004JE002367.  
694  
695 Roberts, J.H., and S. Zhong (2004), Plume-induced topography and geoid anomalies and their  
696 implications for the Tharsis rise on Mars, *J. Geophys. Res.* 109, E03009, doi:10.1029/2003JE002226.  
697  
698 Rouby, H., Greff-Lefftz, M., and J. Besse (2008) Rotational bulge and one plume convection pattern:  
699 Influence on Martian true polar wander, *Earth and Planet. Sci. Lett.* 272, 212-220.  
700  
701 Schultz, P., and A. Lutz (1988), Polar wandering of Mars, *Icarus* 73, 91-141.  
702  
703 Scott, D.H., and K.L. Tanaka (1986), Geological Map of the Western Equatorial Region of Mars, US  
704 Geol. Surv. Scientific Investigations I-1802-A  
705  
706 Shean, D.E., Head, J.W., Fastook, J.L., and D.R. Marchant (2007), Recent glaciation at high elevations  
707 on Arsia Mons, Mars: Implications for the formation and evolution of large tropical mountain glaciers,  
708 *J. Geophys. Res.* 112, E03004, doi:10.1029/2006JE002671.  
709  
710 Skinner, J.A., T.M. Hare, and K.L. Tanaka (2006), Digital Renovation of the Atlas of Mars  
711 1:15,000,000-Scale Global Geologic Series Maps, LPSC XXXVII, abstract #2331.  
712  
713 Solomon, S., et al. (2005), New perspectives on ancient Mars, *Science* 307, 1214-1220.  
714  
715 Tanaka, K.L. (2000), Dust and ice deposition in the Martian geologic record, *Icarus* 144, 254-266.  
716  
717 Tanaka, K.L., and E.J. Kolb (2001), Geologic History of the Polar Regions of Mars Based on Mars  
718 Global Surveyor Data: I. Noachian and Hesperian Periods, *Icarus* 154(1), 3-21.  
719  
720 Tanaka, K.L., Chapman, M.G., and D.H. Scott (1992), Geologic map of the Elysium region of Mars,  
721 US Geol. Surv. Miscellaneous Investigations I-2147  
722  
723 Tanaka, K.L., J. A. Skinner Jr., T. M. Hare, T. Joyal, and A. Wenker (2003), Resurfacing history of the  
724 northern plains of Mars based on geologic mapping of Mars Global Surveyor data, *J. Geophys. Res.*  
725 108, doi:10.1029/2002JE001908.  
726  
727 Tanaka, K.L., and D.H. Scott (1987), Geological Map of the Polar Regions of Mars, US Geol. Surv.  
728 Scientific Investigations I-1802-C  
729  
730 Tanaka, K.L., J.A. Skinner, and T.M. Hare (2005), Geologic Map of the Northern Plains of Mars, US  
731 Geol. Surv. Scientific Investigations I-2888 (<http://pubs.usgs.gov/sim/2005/2888/>).  
732  
733 Watters, T.R., et al. (2007), Radar sounding of the Medusae Fossae Formation Mars: Equatorial ice or  
734 dry, low-density deposits?, *Science* 318, 1125-1128.  
735  
736 Werner, S.C. (2005), Major aspects of the chronostratigraphy and geologic evolutionary history of

737 Mars, PhD thesis, Freie-Universitat Berlin.  
738  
739 Werner, S.C. (in press), The global Martian volcanic evolutionary history, *Icarus*.  
740  
741 White, S.M., J. Crisp, and F.J Spera (2006), Long-term volumetric eruption rates and magma budgets,  
742 *Geochem. Geophys. Geosyst.* 7(3), doi:10.1029/2005GC001002.  
743  
744 Willeman, R. (1984), Reorientation of planets with elastic lithospheres: *Icarus*, vol. 60, pp. 701–  
745 709.  
746  
747 Wilson, L., E.D. Scott, and J.W. Head (2001), Evidence for episodicity in the magma supply to the  
748 large Tharsis volcanoes, *J. Geophys. Res.*, 106(E1), 1423-1433.  
749  
750 Zhong, S. (2009), Migration of Tharsis volcanism on Mars caused by differential rotation of the  
751 lithosphere, *Nature Geoscience* 2, 19-23.  
752  
753 Zuber, M.T., and D.E. Smith (1997), Mars without Tharsis, *J. Geophys. Res.* 102(E12), 28673-28685.  
754  
755 Zuber, M.T., et al. (1998), Observations of the North Polar Region of Mars from the Mars Orbiter Laser  
756 Altimeter, *Science* 282, 2053-2060.

757 **Table 1.** a) (Northern) paleopoles calculated for TPW driven by young volcanic load. Letters refer to  
758 the solutions that are plotted on Figure 6. b) (Northern) paleopoles calculated for TPW driven by  
759 individual volcanic provinces. See Figure 3a for province locations. Only 'large' loads considered. Far-  
760 from-equator solutions are plotted on Figure 5.

761

762 **Table 2.** Best-fitting geologically inferred paleopole locations. OD = Olympia Dome; PB = Planum  
763 Boreum, upper North Polar Layered Deposits (similar extent to that of residual water-ice cap); SC =  
764 Scandia depressions; ST = Scandia mounds; IO = ice outliers; SRC = Southern Residual Cap (CO<sub>2</sub> ice);  
765 SPLD = South Polar Layered Deposits; DAF = Dorsa Argentea Formation. Deviation of youngest polar  
766 deposits from spin axis =  $(2.4 \pm 0.3)^\circ$ . This uncertainty is one-sided for the SRC because atmospheric  
767 effects forced by Noachian topography displace CO<sub>2</sub> precipitation patterns meridian-ward. The final  
768 column is a (subjective) confidence level that each paleopole is due to TPW. *Requirements for a good*  
769 *geologically inferred paleopole:* Asymmetric retreat of formerly more extensive ice sheets is an  
770 alternative explanation for the shape and distribution of Planum Boreum (Fishbaugh & Head, 2001)  
771 and Planum Australe. It is possible that asymmetric sublimation and aeolian erosion has affected the  
772 shape of the Basal Unit plateau (Tanaka et al., 2008) and Planum Australe (Milkovich & Plaut, 2008) to  
773 the extent that their present-day areal centroids are not close to their past areal centroids. Present  
774 outcrop distributions can only be useful as a guide to the past location of the spin axis if either: 1) the  
775 ice-sheet is preserved largely intact; 2) original ice-sheet volume is decimated, but the areal extent of  
776 the plateau is unaltered; 3) the ice sheet undergoes symmetric retreat; or 4) the ice sheet undergoes  
777 asymmetric retreat, but leaves morphological signatures such as moraines, eskers, and kettles that allow  
778 its original extent to be reconstructed. Asymmetric retreat of cold-based ice sheets (for which none of  
779 these conditions need hold) could confound interpretation of the distribution of Martian paleopolar  
780 deposits in terms of TPW. However, the original extent of cold-based high-obliquity ice sheets on the

781 flanks of the Tharsis Montes has been reconstructed using moraines deposited during their incomplete  
782 retreat (e.g., Shean et al., 2007).

783

784 **Table S1.** Load thicknesses. Unit designations are from I-1802AB. For each unit, we either assume a  
785 uniform thickness (a relatively thin late-stage drape over Noachian-Early Hesperian materials), or  
786 truncate the edifices near their base (which assumes that the bulk of the unit is Late Hesperian or  
787 Amazonian). All units are meters (m). Uniform thicknesses are denoted by numbers without appended  
788 parentheses. Parenthetical 'T' denotes edifice truncated at this elevation, and thickness taken to be the  
789 pixelwise ( $\frac{1}{4}^\circ \times \frac{1}{4}^\circ$ ) thickness above that elevation. Negative thicknesses are not permitted. We  
790 modified published geological maps by: 1) assigning  $\frac{1}{4}^\circ \times \frac{1}{4}^\circ$  areas shown on the map as either  
791 'undivided', 'volcano, relative age unknown' or 'crater ejecta' to the nearest dated unit, 2) subdividing  
792 members of the Tharsis Montes formation into Arsia Mons, Pavonis Mons and Ascreaus Mons sub-  
793 members, and 3) following Bradley et al. (2002), subdividing the Medusae Fossae Formation by lobe  
794 rather than by stratigraphic level

795

796 **Figure 1.** Azimuthal equal-area projection centered on 165E, 0N, showing relationship between load,  
797 TPW response, and polar deposits. Grid spacing is  $30^\circ$ , in both latitude and longitude. Red tint is area  
798 of Late Hesperian – Amazonian volcanics (Nimmo & Tanaka, 2005), shown in more detail in Figure 3.  
799 Blue and pink tones are polar and paleopolar deposits, shown in more detail in Figure 6. Yellow spot is  
800 center of Tharsis load, at 248.3E, 6.7N (Zuber and Smith, 1997). Polar wander driven by post-Tharsis  
801 loads of magnitude much smaller than Tharsis, the subject of this paper, lies close to the green line  
802 (Tables 2 and 3), which is within  $7^\circ$  of the great circle perpendicular to Tharsis. Positive loads in the  
803 68E – 248E hemisphere N of the equator, or in the 248E – 68E hemisphere S of the equator, will lever  
804 the spin axis toward the top of the figure, relative to the lithosphere (Figure 4). Loads in the 68E –

805 248E hemisphere N of the equator, or positive loads in the 248E – 68E hemisphere S of the equator,  
806 will lever the spin axis toward the base of the figure, relative to the lithosphere (Figure 4).

807

808 **Figure 2.** Sketch section showing a) south polar and b) north polar stratigraphy, drawn so that left is up  
809 in Figure 1. Principal inferred direction of polar wander is from right to left. Line of section is the green  
810 line in Figure 1; each section runs from 70S, through the pole, to 70S in the opposite hemisphere  
811 (~2400 km). Locally, the Dorsa Argentea Formation extends beyond 70N.

812

813 **Figure 3.** Close-up of region of volcanic loads. a) Uniform load with thickness 100m (total volume  $3.0$   
814  $\times 10^6$  km<sup>3</sup>, of which 77% by volume lies N of equator). Labeled provinces are referred to in Table 1a.;  
815 b) 'Small' load ( $11.2 \times 10^6$  km<sup>3</sup>, 79% ); c) 'Medium' load ( $19.0 \times 10^6$  km<sup>3</sup>, 77%), d) 'Large' load ( $35.4 \times$   
816  $10^6$  km<sup>3</sup>, 79%).

817

818 **Figure 4.** North polar projection showing dependence on latitude and longitude of TPW driven by a  
819 small positive surface load. Vectors show the direction and magnitude of north pole displacement that  
820 would be caused by placing the same load at different geographic locations within the northern  
821 hemisphere. Concentric circles are 0N, 30N, and 60 N. Ratio of maximum TPW angles in plots is 1: 1.1  
822 : 34.1. a) Without Tharsis, and with remnant rotational bulge at equator, the amount of TPW is small,  
823 and any load displaces the pole along the line of longitude that passes through the load. b) Small  
824 Tharsis-driven TPW scenario. The amount of TPW is still small, but in contrast to (a), the direction of  
825 TPW generally has a component perpendicular to the meridian that passes through Tharsis. White  
826 circle is pre-Tharsis pole; black circle is Tharsis location. c) Large Tharsis-driven TPW scenario. The  
827 symbols for Tharsis and the pre-Tharsis pole overlap due to the map projection. TPW is large, but  
828 restricted to directions perpendicular to the line of longitude that passes through Tharsis.

829

830 **Figure 5.** South polar region showing province-by-province paleopoles (Table 1a). 'Large' load, large  
831 TPW scenario. For each province,  $T_e = 100$  km, 200 km and 300 km solutions are at increasing  
832 distances from the pole. See Figure 6b for key to polar geologic units.

833         There is some disagreement about the correct boundary of the Dorsa Argentea Formation. By  
834 using the original boundary of Tanaka and Scott (1987), we adhere more closely to the preferred  
835 boundary of Ghatan & Head (2004) than to the revised boundary of Tanaka & Kolb (2001).

836

837 **Figure 6:** a) North polar region, and b) South polar region, showing:– paleopoles computed from  
838 estimates of young volcanic load (triangles; Table 1a for key); paleopoles inferred from geology  
839 (nested green circles; Table 1a for key); and distribution of polar and paleopolar deposits (tinted areas).  
840 Dark blue line is the convex hull of the Scandia mounds. Green dashed lines define error envelopes  
841 based on the deviation of the youngest polar deposits from the current spin axis ( $2.4 \pm 0.3^\circ \equiv 140 \pm 20$   
842 km, the 'proxy error' discussed in the text). We estimate that the additional error in assigning a centroid  
843 locations to a paleopolar deposit ('measurement error') is comparable to or greater than this error, and  
844 we show this additional error by the outer green circles. Ice outliers are probably young  
845 (contemporaneous with upper Planum Boreum or younger), but are shown because they might be  
846 obscuring older deposits.

847

848 **Figure 7.** One possible synthesis of Martian volcanic and polar history using TPW constraints and the  
849 assumption that areal centroids of polar deposits track the spin axis. Degree of confidence increases  
850 with observed offset. The contribution of internal dynamics to TPW is assumed to be small (see §6.3  
851 for a discussion of this assumption). Other less simple syntheses are also consistent with the data.  
852 Elevations are not to scale. a) Deposition of Dorsa Argentea Formation (DAF) during Hesperian.

853 Ongoing volcanism at Elysium (Ely). b) Loading in Quadrants 1 or 3 (e.g. by Elysium or proto-  
854 Olympus Mons, Oly; Figure 5) shifts pole by 5.9 degrees in great circle 90 deg from Tharsis in a  
855 meridian-ward sense. Deposition of Scandia (Sc) materials intercalated with loading, Basal Unit (BU)  
856 postdates loading. c) Further loading in Quadrants 1 or 3 (e.g. by waning Elysium flows, Olympus  
857 Mons activity or Arcadia young flood lavas; Figure 5) drives further polar wander of 7.5 degrees in  
858 meridian-ward sense. Deposition of Promethei Lingular Lobe of SPLD. d) Loading in Quadrants 2 or 4  
859 (most likely by Tharsis Montes, TM; Figure 5) drives polar wander of 5 degrees in anti-meridian sense.  
860 Deposition of Planum Boreum (PB) intercalated with or subsequent to loading. Deposition of the  
861 geologically very young Southern Residual Cap (SRC).

862

863 **Figure 8.** Magnitude of TPW versus total volume of late Hesperian and Amazonian volcanism, for a  
864 range of assumptions about lithospheric thickness and orientation of fossil rotational bulge. Colored  
865 bars show range of magnitudes/volumes for which computed TPW matches geologically inferred  
866 wander to within  $\pm 1^\circ$ . Red vertical lines are small, medium and large loads. The South Polar Layered  
867 Deposits are not plotted because their offset cannot be accommodated by a 'proportional' volcanic  
868 history.

a) Combined surface loads			Tharsis formed close to equator			Tharsis formed far from equator		
Load	Volume (x 10 <sup>6</sup> km <sup>3</sup> )	Center of volume	Te = 100km	Te = 200km	Te = 300km (a)	Te = 100km (b)	Te = 200km (c)	Te = 300km (d)
'Small' (A)	11.2	17.4N 220.5E	89.8N 181.7E	89.6N 186.1E	89.5N 185.2E	83.8N 161.1E	79.3N 162.3E	77.3N 163.0E
'Medium' (B)	19.0	15.3N 220.3E	89.7N 183.4E	89.4N 181.2E	89.2N 180.9E	80.0N 161.8E	73.0N 162.7E	69.3N 163.3E
'Large' (C)	35.4	18.0N 217.8E	89.3N 180.5E	88.7N 181.3E	88.4N 180.6E	71.5N 162.7E	62.0N 164.9E	57.7N 165.9E
Uniform drape, 100m thickness	3.0	20.8N 214.8E	89.9N 169.4E	89.9N 181.2E	89.9N 177.2E	88.0N 159.4E	86.3N 160.7E	85.4N 160.4E
Uniform drape, 1000m thickness	29.6	20.8N 214.8E	89.4N 175.6E	88.9N 175.0E	88.6N 175.2E	72.5N 162.1E	61.0N 164.0E	56.7N 165.0E
b) Each province, 'large' load			Tharsis formed close to equator			Tharsis formed far from equator		
Load	Volume (x 10 <sup>6</sup> km <sup>3</sup> )	Center of volume	Te = 100km	Te = 200km	Te = 300km (a)	Te = 100km (b)	Te = 200km (c)	Te = 300km (d)
Elysium province	6.6	22.3N 152.5E	89.6N 154.8E	89.3N 156.1E	89.1N 156.4E	76.0N 160.1E	64.8N 161.2E	59.3N 162.0E
Medusae Fossae province	2.2	1.4S 201.1E	90.0N 335.4E	90.0N 305.5E	90.0N 305.5E	89.4N 335.4E	89.4N 335.4E	89.4N 335.4E
Young flood lavas	4.1	33.1N 187.1E	89.8N 174.3E	89.7N 167.3E	89.6N 169.8E	84.6N 160.3E	80.3N 160.2E	77.2N 160.8E
Olympus province	6.1	19.4N 224.9E	89.8N 198.5E	89.7N 197.2E	89.6N 196.1E	85.6N 162.9E	81.8N 163.4E	80.4N 163.6E
Tharsis Montes province	10.0	3.5N 248.5E	89.9N 304.4E	89.9N 304.5E	89.8N 309.4E	87.7N 335.0E	86.0N 334.7E	85.2N 335.2E
Alba province	4.6	41.3N 249.0E	89.9N 255.2E	89.8N 252.5E	89.7N 251.7E	89.3N 303.0E	89.1N 287.1E	89.0N 280.0E
Syria	1.9	15.9S	90.0N	89.9N	89.9N	88.8N	87.9N	87.9N

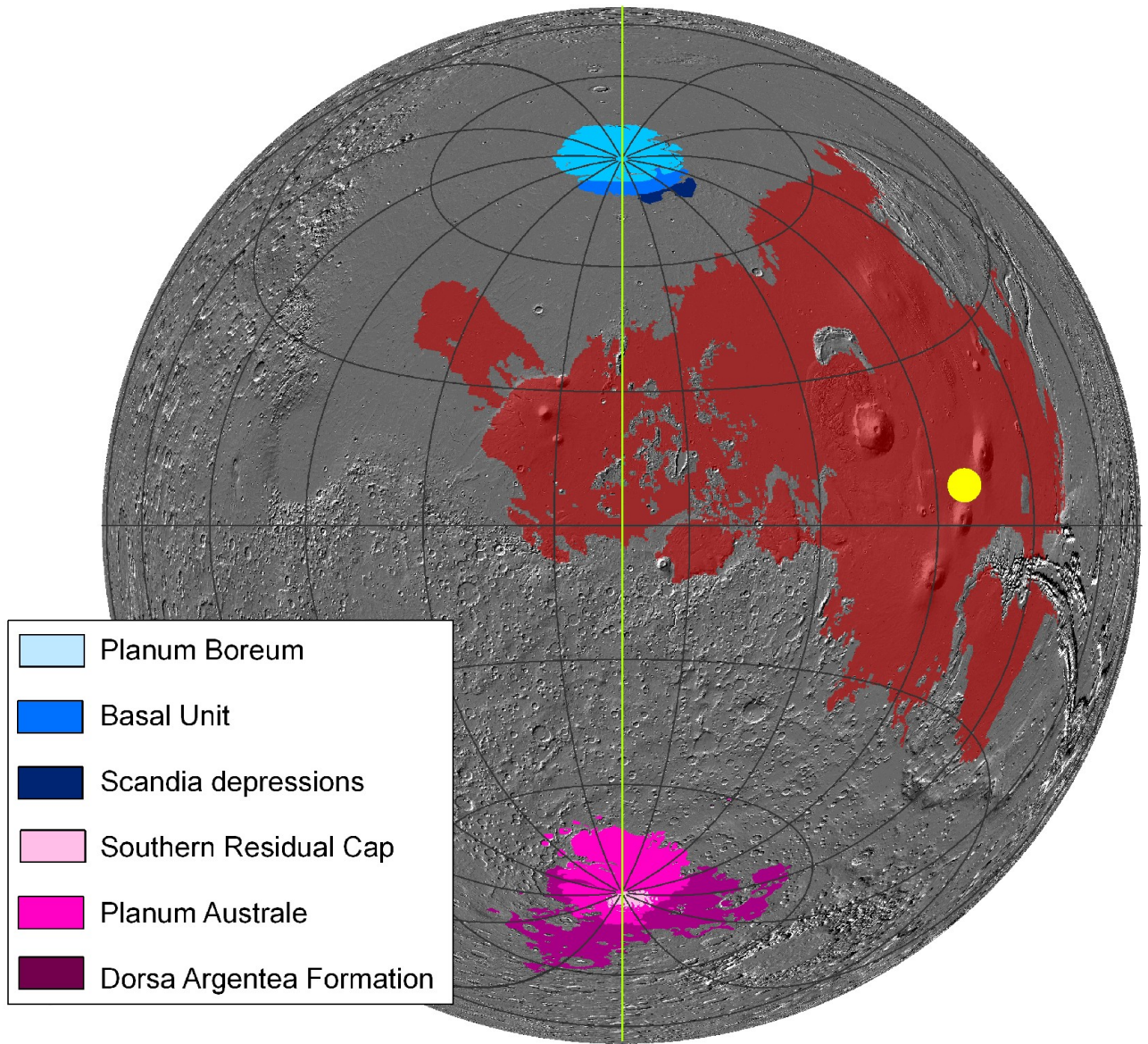
province		266.5E	122.5E	112.7E	112.7E	155.3E	154.2E	154.2E
----------	--	--------	--------	--------	--------	--------	--------	--------

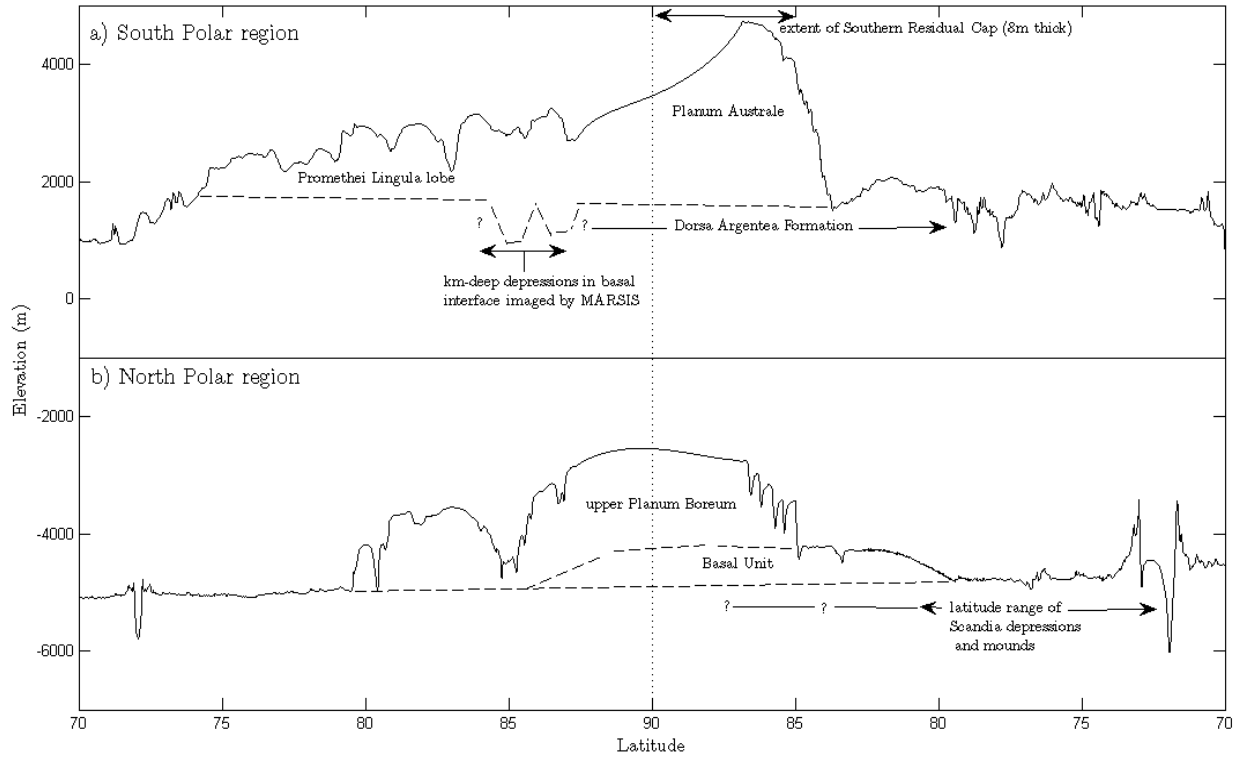
Crater-retention age	Polar material	Mask (younger materials)	Best fit pole location	(Relative) Confidence that paleopole is due to TPW?
<b>Northern hemisphere</b>				
<i>Without ice outliers</i>				
1. Late Amazonian	PB	–	87.9N 1.4E	Low to Moderate
2. Late Amazonian	OD	PB	87.6N 181.2E	Moderate
3. Early Amazonian	SC	PB, OD	85.0N 206.8E	Low
4. Early Amazonian	SC, ST	PB, OD	81.3N 198.6E	Very Low to Low
<i>With ice outliers</i>				
Late Amazonian?	IO	PB, OD	84.6N 160.9E	Ice outliers overlie SC and ST, but age relative to PB is uncertain
Early Amazonian?	IO, SC	PB, OD	83.7N 185.5E	
Early Amazonian?	IO, SC, ST	PB, OD	81.3N 189.7E	
<b>Southern hemisphere</b>				
5. Upper Amazonian	SRC	–	87.3S 315E	n.a. (see §1)
6. (?Middle) Amazonian	SPLD	–	84.3S 162.7E	Moderate
7. Late Hesperian	DAF	SPLD	82.1S 335.9E (variable cap radius) <i>81.3S 302.1E (fixed cap radius)</i>	High

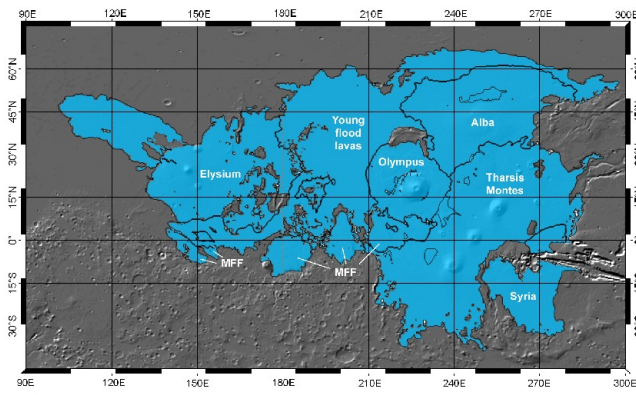
Unit desig.	Description	Unit thickness or truncation elevation (m)			Notes
		'Small'	'Medium'	'Large'	
<i>Elysium Province</i>					
Hhet	Hecates Tholus Fm.	-3000 (T)	-3000 (T)	-3500 (T)	Qualitative backstripping following Tanaka et al. (1992)
Ael1	Elysium Fm., member 1	500	1000 (T)	-3500 (T)	
Ael2	Elysium Fm., member 2	2500 (T)	2500 (T)	-3500 (T)	
AHat	Albor Tholus Fm.	-1000 (T)	-1000 (T)	- 3500 (T)	
<i>Medusae Fossae Formation</i>					
Combined lower, middle and upper members of Fm.	W lobes	500	- 2700 (T)	-2700 (T)	Largely following Bradley et al. (2002).
	C lobes	500	-2400 (T)	-2800 (T)	
	E lobes	500	-2000 (T)	-3000 (T)	
	Far E lobe	500	+500 (T)	-500 (T)	
<i>Young flood lavas</i>					
Ael3-4	Elysium Fm., members 3-4	100	200	500	'Small' values from SHARAD and MARSIS subsurface contacts
Achu	Younger channel system material, undivided	75	300	1000	
Aa1	Arcadia Fm., member 1	150	200	500	Not between -55 and +10 deg E
Aa2	Arcadia Fm., member 2	50	100	200	'Small' values from SHARAD and MARSIS subsurface contacts
Aa3	Arcadia Fm., member 3	70	100	500	
Aa4	Arcadia Fm., member 4	30	100	200	
Aa5	Arcadia Fm., member 5	30	100	200	Only between -180 and -150 deg E
Achp	Younger	30	30	100	'Small' value from

	flood-plain material				SHARAD and MARSIS subsurface contacts
<i>Olympus Mons province</i>					
Aoa1	Olympus Mons Fm., aureole member 1	1000	1000	1000	
Aoa2-Aoa4	Olympus Mons Fm., aureole member 2 – member 4	1500	1500	2200	
Aos	Olympus Mons Fm., shield member	3000	+0 (T)	- 2000 (T)	
Aop	Olympus Mons Fm., plains member	500	1500	2500	
As	Slide material	3000	+0 (T)	- 2000 (T)	Only between -128 E and -140 E. As Aoa2-4
Ae	Eolian deposits	1500	1500	2200	Only between -130 and -150E. As Aoa2-4.
<i>Tharsis Montes province</i>					
AHt3 + At6 + As	Arsia	+ 8000 (T)	+ 6000 (T)	+ 4000 (T)	
	Pavonis	+ 5000 (T)	+ 4000 (T)	+ 2000 (T)	
	Ascraeus	+ 4000 (T)	+ 2500 (T)	+ 0 (T)	
	“marginal”	100	250	250	
At5	Tharsis Montes Fm., member 5	200	500	500	
At4 (distal)	Tharsis Montes Fm., member 4	100	250	500	
<i>Alba Patera province</i>					
Aau	Alba Patera Fm., upper member	+4500 (T)	+2000 (T)	+0 (T)	Late Hesperian apron and Earliest Amazonian summit according to

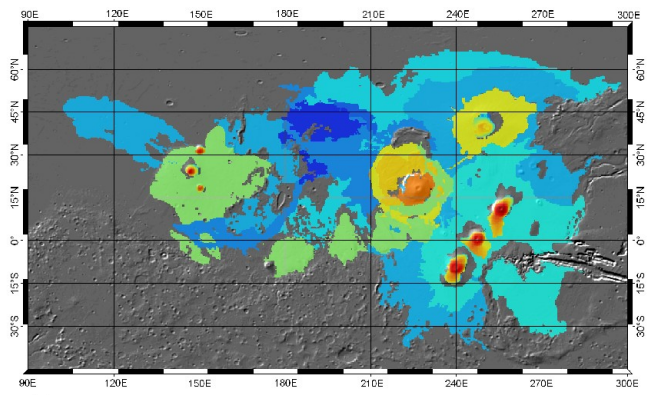
Aam	Alba Patera Fm., middle member	1000	+2000 (T)	- 1000 (T)	Ivanov and Head (2006)
Hal	Alba Patera Fm., lower member	100	200	500	
<i>Syria province</i>					
Hsl	Syria Planum Fm., lower member	200	500	1000	
Hsu	Syria Planum Fm., upper member	200	500	1800	
<i>Other</i>					
AHcf	Ceraunius Fossae Formation	200	450	1000	
“Nf”	Highly-deformed terrain materials	200	500	2500	Adjacent to AHcf only
Ht1-2	Tharsis Montes Fm., members 1-2	100	200	500	
Apk	Knobby plains material	100	200	500	Only near to Tharsis Montes



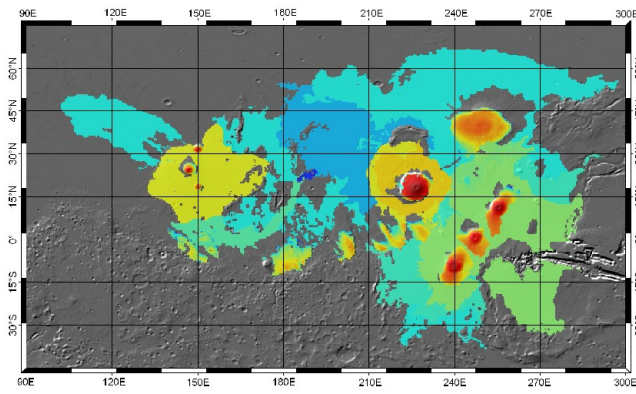




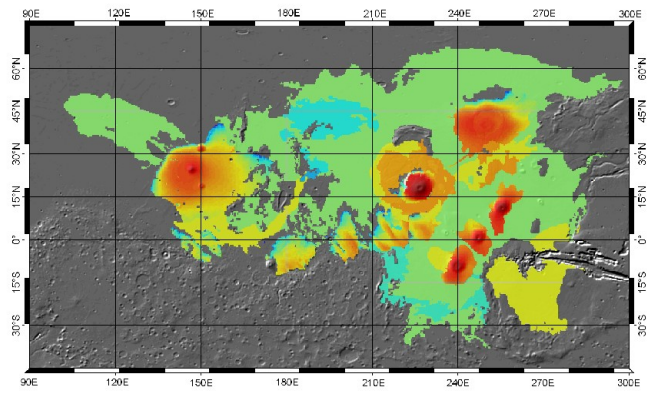
a)



b)



c)



d)

